Progress In Electromagnetics Research M, Vol. 47, 99–110, 2016

In-Situ Monitoring Method for Direction Finding Antennas

Lama Ghattas[1, *], Serge Bories[1], Dominique Picard[2], Philippe Pouliguen[3], and Patrick Potier[3]

Abstract—Antenna arrays for direction finding (DF) are usually designed and tested in controlled environments such as anechoic chambers. However, antenna pattern may change significantly when antennas are placed in their operational environment. In such perturbing close context, the antennas calibration validity becomes a major issue which can lead to DF performance degradation and costly recalibration process. This paper presents an innovative design and implementation of a non-disturbing solution for quasi-real time antenna monitoring. The proposed system is based on optically modulated scattering (OMS) technique. Its capacity to detect the presence of various types of obstacles, which significantly perturb the antenna radiation pattern, is evaluated. A relation between monitoring mode and DF mode measurement signals is established. Finally, a design and sizing of the overall system is proposed.

1. INTRODUCTION

In telecommunications and radar fields, antenna measurements are typically performed in a controlled environment (usually in an anechoic chamber, without scatterers, obstacles and parasitic reflections) to ensure that the antennas meet specifications. Moreover, in a number of applications, these measurements are also used to calibrate the antennas far-field response requested by the antenna processing algorithms.

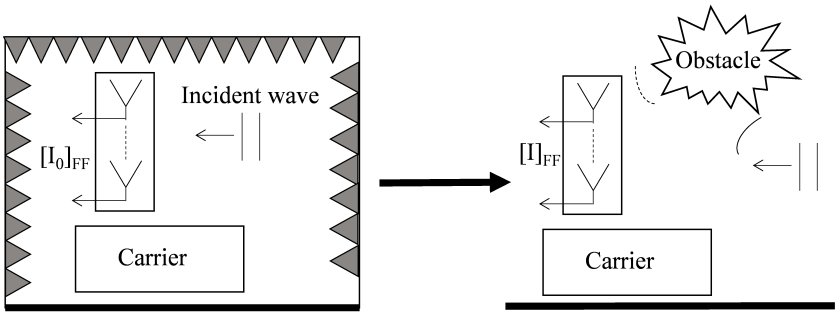

Figure 1. Antenna array calibration and in-situ configuration.

This is particularly relevant for Direction Finding (DF) applications for which antenna model errors are usually a major source of performance degradation. Fig. 1 shows a typical calibration process of an antenna array mounted on a carrier. The calibration table is constituted by the responses of each antenna excited by a plane wave. The calibration table can be presented as a four-dimensional matrix depending on frequency, incidence angles and number of antennas [1]. It is established in a controlled

Received 17 November 2015, Accepted 27 January 2016, Scheduled 30 March 2016
* Corresponding author: Lama Ghattas (ghattas.lama@gmail.com).
[1] CEA-LETI Grenoble, France. [2] CentraleSupelec, Paris, France. [3] DGA, Paris, France.

environment and remains in the memory of the DF system. Once Direction Finding Antennas (DFA) are deployed in their operational environment, closed obstacles (not previously considered) may affect the DFA radiation pattern and thus the validity of their calibration. To detect the variable obstacles that disrupt the nominal DFA calibration, in this study we propose to compare the received current response to an incident EM wave for the two following cases: nominal response $[I_0]_{FF}$ and in-situ response $[I]_{FF}$ (Fig. 1), for which scatterers and obstacles reflection are taken into account. Two modes are now sequentially considered: the classical DF mode and monitoring mode. Notice that the embedded monitoring device should not disturb the DF performance. Several reported works deal with prediction or detection of in-situ antenna calibration robustness. In [2], the performance of DFA was investigated with a calibration table simulated with a 3D EM simulator. A good agreement was shown between measured and simulated calibration tables but with no real time update. In [3], it is shown that a single antenna pattern and coupling between antennas are not sufficient for predicting the array manifold. This is mainly explained by the influence of the antenna structure scattering. A real-time diagnosis tool based on a slotted coaxial cable probe placed closed to transmitting phased array radar is evaluated in [4]. This interesting solution could only detect failure or obstacle perturbation inducing a near-field modification where the probe is placed (bottom of the aperture). Furthermore, similar optimization steps for correcting the radiation pattern of antenna are proposed. In [5], a concept of an effective radiation pattern computation taking into account the distorsions induced by radio channels for a LTE Wireless system is proposed. The overall objective of this work is to propose a solution for detecting near-field deviation between in-situ antenna performance and nominal behavior. This will provide guidance to specify restricted areas around the antenna governed by the accuracy of the system. The Optically Modulated Scatterer Technique (OMS) is a very promising method of electromagnetic field measurement leading to minimum perturbations [6]. Introduced in the 1950s [7], this method of radio-frequency electromagnetic field measurement is now more commonly used than in the past due to the current technological progress, which allows exploiting its advantages. This technique has been successively applied to the measurement of antenna pattern [8, 9], evaluation of the performance of microwave absorbers [10], source location estimation [11] microwave tomography [12] and microwave near-field imaging for cancer detection [13]. In these works, probes are generally optimized and characterized to operate over a narrow frequency band. In this work, the OMS technique is chosen as a low perturbation solution to diagnose DFA calibration. The presence of variable obstacles is detected by monitoring the change in the level of the scattered power by the probe (as described in Section 3.1). Increasing the backscattering power is a key objective while keeping a low level of disturbance. In our study, the DF system has very wide band, to support (VHF-UHF) spectrum monitoring application. This paper proceeds as follows. In Section 2, the benefit of an in-situ monitoring system for DFA is presented. The principle of the selected approach and testbed component characterization is detailed in Section 3. The influence of obstacles near the antenna is shown in Section 4. A relation between the OMS signal level probe variations induced by the presence of the obstacle and the degradation of the performance of DF is presented in Section 5.

2. BENEFIT OF AN IN-SITU MONITORING SYSTEM FOR DFA

In order to highlight the benefit of an in-situ measurement system, the application of DFA mounted above a vehicle is studied [14].

2.1. Model of DF System

DF system allows assessing the angle of arrival of an incident EM wave on an antenna array by using a DF algorithm. The choice of this application to demonstrate the benefit of a quasi-real time monitoring of antenna performance is relevant so that a precise estimation of direction of arrival requires a detailed knowledge of the complex characteristics of antennas and this over several decades of frequency. Indeed, modern DF algorithms are sensitive to array manifold model errors. A numerical model of the whole receiver chain has been implemented (Fig. 2). The characteristics of antenna arrays on their carrier and the presence of close scatterers are modeled using a 3D EM simulator FEKO. It is based on the Method of Moments (MoM) which is applicable to problems involving currents on metallic and dielectric

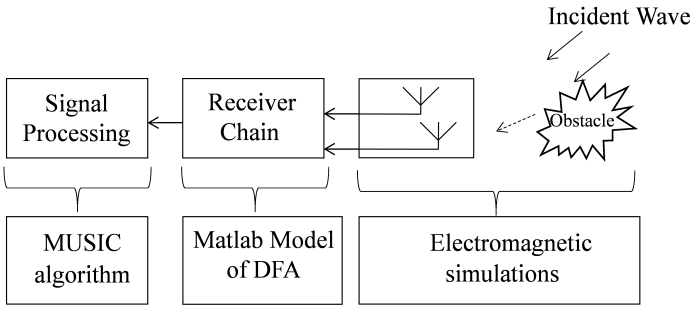

Figure 2. Model of direction finding system and signal processing channel.

structures and radiation in free space [15, 16]. The complex response (ratio of the induced current to a given incident field) of each antenna for every angle and every frequency constitutes simulated calibration tables, taking into account disturbing elements such as reflections, mutual coupling, radiation pattern of antennas and all disturbing elements (mast,cables, carrier ...). The RF reception chain (cables, RF amplification, filtering, and addition of thermal noise) is implemented in Matlab. The MUSIC algorithm is implemented for the DOA estimation. It is based on the comparison between the received signals by the antennas and those stored in the calibration table [1]. The expected DOA accuracy is an important parameter of any DF system. It depends on implementation, imperfections, interference, signal-to-noise (SNR) ratio and so forth. To estimate the precision and allow the comparison between different configurations, the minimum signal to noise ratio ($SNR_{\min}$) at the receiver input to obtain a root mean square error (RMS) less than 2° on the incidence direction is considered. This 2° value is the typical accuracy for goniometer. The used metric has the advantage to be global and compact.

2.2. Influence of Scatterers

2.2.1. Influence of Variable Scatterers

The disturbances due to the presence of the vehicle can be compensated during the "first factory" calibration, including the vehicle. However, when the antenna array is placed in its real operating environment (in-situ), it is potentially affected by near scatterers, which may affect the calibration. In this section, non-stationary obstacles are considered; that is closed context configuration potentially modified within the same mission (roof hatch). As an example, a metallic rod (3 mm diameter and 1 m length) emulating a whip antenna is positioned in a corner of the roof of the vehicle (Fig. 3). A plane wave with vertical polarization impinges the DFA with an angular step of one degree. The antennas are made of copper and terminated in a matched load of 50 Ω; the vehicle is made of perfect conductor. A soil with relative permittivity of 15 and conductivity of $2e-2$ S/m is modeled under the vehicle. Initially, five elements (25 cm height dipoles) uniformly spaced on a circular array with a diameter of 1 m are positioned 4 m above the roof of the vehicle. The simulations were done using 8 cores per physical CPU. The number of basis function for MoM is 19062. Symmetry conditions are not used in this simulation because of the presence of the vehicle.

The simulations are conducted in two cases: with and without the metallic rod. Fig. 4 shows the evolution of $SNR_{\min}$ for a configuration with the metallic rod calibrated with nominal configuration for the same distance h of DFA from the roof. The $SNR_{\min}$ to obtain 2° of RMS error decreases with frequency due to the increase of the electric size of the antenna array (Cramer Rao Bound [17]). When the DFA is at 4 m from the roof, we can retrieve the same performances as in the absence of the metallic rod (maximum difference of 1 dB). However, when the DFA is only at 1 m from the roof, strong degradations are observed at resonance frequencies of the monopole. The resonance frequency of the metallic rod at $3\lambda/4$ (225 MHz) corresponds to the strong oscillation at 225 MHz. For higher resonances, the effect is less significant.

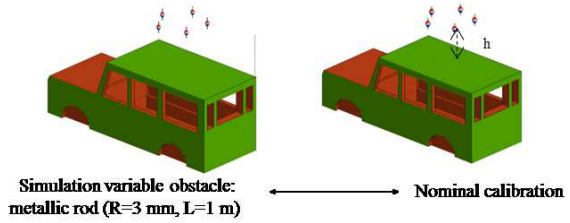

Figure 3. Configuration of DFA (array of 5 dipoles) placed on a vehicle with and without metallic rod.

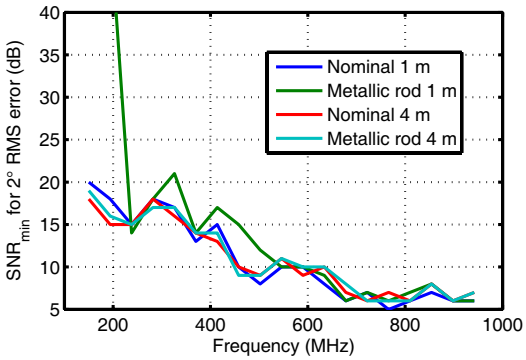

Figure 4. Evolution of $SNR_{\min}$ of DFA in the presence of metallic rod.

3. OMS PROBE DESIGN

3.1. Proposed Monitoring System

According to the foregoing, the importance of developing an in-situ measurement system around the DFA array is demonstrated. Because of the difficulty of accessing the far field of the antenna in-situ, the proposed system consists in monitoring the near field of the Antenna under Test (AUT) (see Fig. 5). A number of transmitters (probes array) are placed around the DFA. A near-field calibration is performed. In this new calibration, the wave is generated successively by each of the probes, which operates in the transmit mode. The response of the antenna array is stored for each probe stimulus. A new table called "monitoring table" is then set and stored on the system memory. Once placed in-situ, the monitoring system can transmit with a low duty cycle, which depends on the context stationarity. The current induced in each antenna of the DF array $[I]_{NF}$ is measured and compared with $[I_0]_{NF}$. The difference $\Delta[I]_{NF}$ can be assessed for each probe. If the difference is greater than a given threshold, an alarm is raised to alert the user to the presence of an obstacle affecting the performance of direction finding. Note that the proposed monitoring system is taken into account in the first factory calibration of the far field.

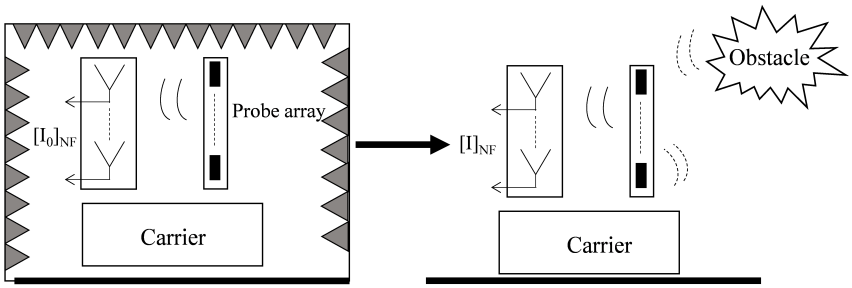

Figure 5. Proposed system for DFA monitoring.

3.2. Dimensioning of OMS Probe

The photodiode selected to load the OMS probe is the PDCS30T manufactured by Albis [18]. This component is selected due to its high impedance variation as a function of optical input level. In practice, a limited number of antenna types, including dipoles, loops, horns, and microstrip antennas, have been used as MST probes. The leading criterion to select the type of antenna is to minimize the interaction between the probe and the AUT [6].

3.2.1. OMS Harmonic Link Budget Model in the Near Field

In order to predict the OMS power budget of an antenna, a formulation has been proposed in [19]. It consists of treating separately the linear part (transmission field links) and nonlinear part (photodiode impedance modulation). The received spectrum contains a strong signal at the carrier frequency F_c and harmonic spectral lines at $F_c \pm nF_m$. Eq. (1) shows the Fourier coefficients for the nth sideband of the voltage at the receiving antenna port:

$$V_{n,\sin} = \begin{cases} \dfrac{4}{n\pi} Z_{rs} Z_{st} \left(\dfrac{1}{Z_{ss} + Z_{OFF}} - \dfrac{1}{Z_{ss} + Z_{ON}} \right) I_{Tx} & \text{if } n \text{ odd} \\ 0 & \text{if } n \text{ even} \end{cases}$$
$$V_{n,\cos} = 0 \tag{1}$$

where Z_{rs} describes mutual impedance between AUT and OMS probe, Z_{st} mutual impedance between transmitter and OMS; Z_{ss} is the probe impedance; Z_{ON}, Z_{OFF} represent the photodiode impedance in the ON and OFF states, respectively; I_{Tx} is the current at T_x antenna port. The link power budget is then computed by evaluating the ratio between powers at the receiving and transmitting antennas ports P_e and P_r.

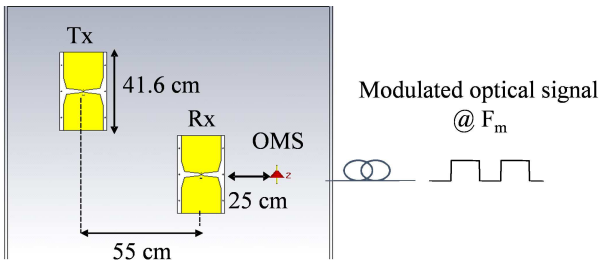

Figure 6. Simulated and measured configuration for OMS power budget evaluation.

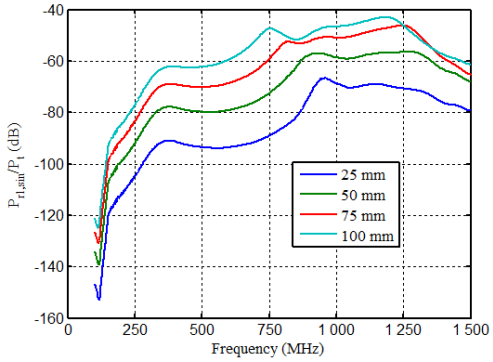

Figure 7. Comparison of simulated OMS power budget for different probe lengths.

In order to select the optimal probe length in the frequency band 150 MHz–1 GHz, the OMS power budget for a bistatic setup with different lengths of probe (25 mm, 50 mm, 75 mm and 100 mm) is computed. Two identical Ultra Wide Band (UWB) bow-ties operating in the band [250 MHz–1 GHz] are used as transmitting and receiving antennas (Fig. 6). The simulation is done with CST MWS. The probe is a planar dipole etched on an FR4 substrate. The first UWB antenna is used as an auxiliary antenna (Tx) and the other as an AUT (Rx). The results (Fig. 7) show that the scattering by the probe is increased when the probe is longer because the sensitivity of a dipole increases with the effective height. For a 10 cm dipole probe, the OMS power budget is greater than −60 dB for frequencies above 400 MHz. More generally, for a given probe length, there is a strong decrease of the OMS power budget when the frequency decreases (in other words, when the antennas are electrically small (less than $\lambda/6$)). Between 25 mm and 100 mm of probe length, the power budget is increased by about 30 dB.

4. DETECTION OF OBSTACLES

Classical backscattering methods are used for antenna characterization [20, 21]. These methods are extremely sensitive to the environment clutter since the backscattering is at the same frequency as the transmission. In OMS technique, the probe tags an EM field at its position; this can be seen as a transmission at $Fc \pm nFm$ between the probe and the monitored antenna. Thus, this method is less sensitive to the environment. Moreover, this method provides less disturbing measurement, thanks to the quasi-nonmetallic OMS probe. In order to demonstrate the efficiency of this method for obstacles

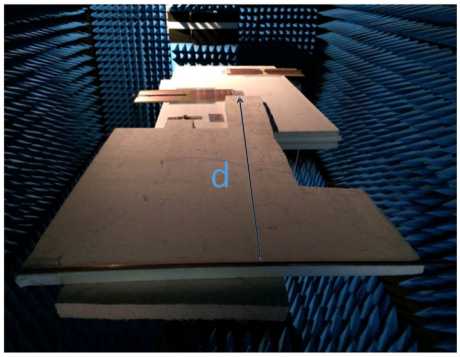

Figure 8. Metallic rod added to the nominal configuration of measurement.

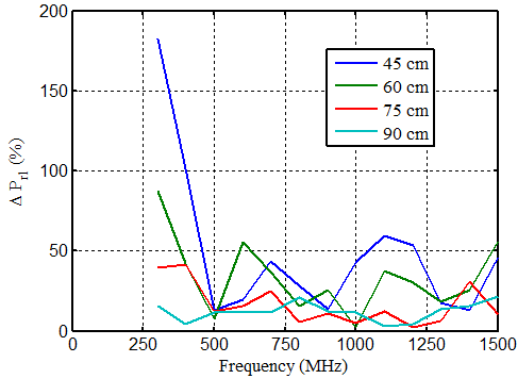

Figure 9. Measured variations of ΔP_{r1} due to the presence of the metallic rod regarding frequency and distance from AUT.

detection, a cylindrical metal rod emulating a whip antenna (diameter of 3 mm and length of 1 m) is placed at different distances from the AUT (Fig. 8).

The presence of the obstacle is observed through the variation of the received power at the first OMS harmonic in the presence and absence of the metallic rod.

$$\Delta P_{r1}(\%) = 100 \left| \frac{P_{rx} - P_{rx0}}{P_{rx0}} \right| \tag{2}$$

where P_{rx0} represents the 1^{st} harmonic scattered power in the nominal configuration (in the presence of PVC support and the plate of polystyrene foam) and P_{rx} the first harmonic scattered power in the presence of the metallic rod. Fig. 9 shows the variation of scattered power at F_c-F_m due to the introduction of the metallic rod and according to the distance d from AUT. The deviation is computed for $d = 45$ cm, 60 cm, 75 cm, 90 cm and 1.1 m. The results show that the deviation decreases when the metallic rod is far from the AUT (deviations less than 20% for distances greater than 75 cm). It reaches a maximum value at 300 MHz. The observed oscillations on the curves are due to the changes in the characteristics of the obstacle (resonance frequency) and the antennas regarding frequency. Oscillations are also present because of the frequency dependence of the phase difference between the signal diffracted by the obstacle and the signal directly transmitted from one antenna to another.

5. RELATION BETWEEN THE MEASURED SIGNAL IN THE MONITORING MODE AND THE ACCURACY OF THE DF MODE

The purpose of this part is to compare the results between the measured deviation in monitoring mode and the deviation of the far field used in DF mode.

5.1. General Considerations

The first idea for the processing of the measured near field in monitoring mode is to realize a near-field to far-field transformation so as to obtain the present radiation pattern. For that it is necessary to measure the near field on a surface, a cylinder for example. This measurement surface is close to the goniometer antenna, and generally the obstacles are outside this surface. The radiation sources are located both inside (DFA and eventually some obstacles) and outside (other obstacles) the surface of measurement. Interior sources generate only divergent waves while external sources generate also convergent waves corresponding to different modes. Measuring two tangential components of the electric field and magnetic field can separate these two types of radiation sources in term of modal expansion. But the obtained modal expansion for the field radiated by the external obstacles does not allow the evaluation of the far field of these sources. In other words, the influence of obstacles lying inside the

surface and only changes of internal sources due to external obstacles can be evaluated on the far field [22]. For this reason, only significant variations of the detected field by OMS probe are assessed in this work. In the following for the sake of simplicity, only one dimension circular probes array is considered. The probes are positioned on a circle with an angular sampling step l defined by $l = \frac{\lambda}{2R_{\min}}$ [6]: where $R_{\min}$ is the radius of the smallest circle, concentric with the measurement circle, in which the DFA can be included. The DFA is a circular array ($R_{\min} = 55\,\text{cm}$), and the probes array is placed at 25 cm concentrically away from the DFA so that the measurement circle radius $R_{meas} = 80\,\text{cm}$. The minimum number of probes required to meet an angular spacing of 20° in the frequency band 150 MHz–1 GHz is 18. A dipole antenna T_x (25 cm length) is positioned 25 cm above the horizontal plane of the receiving DFA array (R_{xi}, $i = 1 \ldots 5$). The probes array $S_j (j = 1 \ldots 18)$ is placed at 80 cm from the center of the DFA.

5.2. Monitoring Mode Versus DF Mode

5.2.1. Different Types of Obstacles

Different types of non-predictable obstacles are added to the simulated configurations. The obstacles can be sorted depending on their distance to the vehicle and whether they intersect the DFA horizontal plane or not (see Table 1).

Table 1. Classification of obstacles.

	On the vehicle	10 m behind the vehicle
In the DFA horizontal plane	Metallic rod	Another vehicle
Out of the DFA horizontal plane	Open roof hatch (1 m length, 0.5 m width)	Street lamp (10 cm radius and 5 m length)
		Metallic board (2 m length, 2 m width, and 5 cm depth)

5.2.2. Monitoring Mode

In this mode, the T_x antenna illuminates the probes array. Each probe S_j scatters a signal on the receiving antennas R_{xi}. The coupling between T_x antenna and the probe S_j is $C_{S_j - T_x}$, and the coupling between the probe S_j and R_{xi} is $C_{R_{xi} - S_j}$. The coupling between the antenna R_{xi} and T_x antenna through the probe S_j is $C_{ij} = C_{S_j - T_x}\, C_{R_{xi} - S_j}$. First, a simulation for the nominal case of the system in the presence of probes array and carrier is carried on. Then, couplings in perturbed case are computed by adding one of the different obstacles to the simulation. The ratio (ΔOMS) between the nominal case and the perturbed case is then computed according to the frequency:

$$\Delta OMS_j(\%) = 100 \sqrt{\sum_{n=1}^{n_f} \sum_{i=1}^{n_a} \frac{1}{n_f n_a} \frac{|[C_{ij}]_n - [C_{0ij}]_n|^2}{|[C_{0ij}]_n|}} \tag{3}$$

where $[C_{0ij}]$ and $[C_{ij}]$ represent the coupling coefficients between antennas without and with an obstacle, respectively, and n_f represents the number of frequencies, n_a the number of antennas.

Figure 10 shows a comparison of the difference between nominal and perturbed cases for the OMS coupling mentioned above as function of the position of the probe. The ratios over R_{xi} antennas are averaged. The curves are flat except for the rod which varies as a function of the probe number. It is because the rod is closest to the DFA. Several phenomena are observed:

(i) When the obstacle is on the vehicle, the degradation by an obstacle in the DFA horizontal plane (ex. Rod obstacle) is greater (6.5% mean over the probes) than that of an obstacle outside this horizontal plan (4.9% mean). The closest probe to the obstacle is most affected (probe N°16).

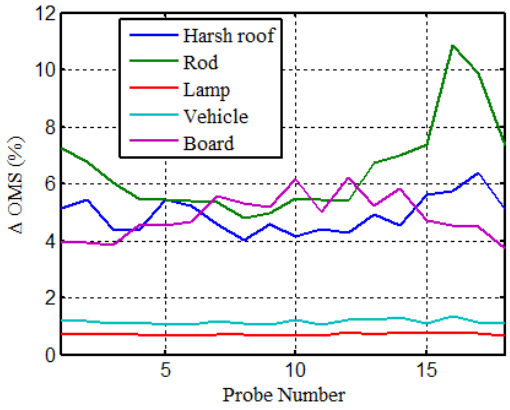

Figure 10. Comparison of simulated OMS coupling ratios for different types of obstacles for each of the probes.

(ii) When obstacles are out of the vehicle, the degradation depends on their radar cross section. A mean difference of 4.9% is observed for the board. For the street lamp and the other vehicle, the differences are less than 2%.

5.3. DF Mode

5.3.1. Received Currents by DFA

From receiving simulations with plane wave excitation for each azimuth degree, the current amplitude and phase on each antenna for every azimuth and every frequency are obtained. These data are stocked in the calibration table and used for DF estimation. The deviation between the received currents with and without different obstacles is computed according to Eq. (4):

$$\Delta I_{FFi}(\%) = 100\sqrt{\sum_{n=1}^{n_f}\sum_{j=1}^{n_s}\frac{1}{n_f n_s}\frac{|[I_{FF}]_{ij_n} - [I_{0FF}]_{ij_n}|^2}{|[I_{0FF}]_{ij}|_n}} \tag{4}$$

where $[I_{0_{FF}}]$ and $[I_{FF}]$ represent received currents by R_{xi} antennas without and with an obstacle, respectively, and n_f represents the number of frequencies, n_s the number of probes. Fig. 11 shows a comparison of the difference between nominal and perturbed cases for received currents by DFA. The ratios over S_j probes are averaged. The standard deviation is calculated on the various points of each curve in Fig. 11 and is normalized by the average value of those points. The normalized standard deviation is indicated near each curve in Fig. 11. When the obstacle is out of the horizontal plane of DFA, the disturbance is almost uniform for the 18 probes with a deviation less than 5%. In the case of an obstacle in the horizontal plane of DFA, the disturbance is greater than 8%. The three curves giving the most correct azimuths in Fig. 12 are those with the weakest normalized standard deviation in Fig. 11 (Vehicle, Lamp and Board).

5.3.2. Proportion of Correct Azimuths at a Fixed SNR

A second DF metric is also considered. The proportion of correct azimuths is the number of azimuths, which provides a RMS error less than 2° at a fixed SNR of 25 dB, divided by the total number of azimuths. This 25 dB threshold is fixed to ensure that the DFA is working well in the selected frequency band (Fig. 3). Fig. 12 shows the proportion of correct azimuths regarding frequency in the presence of different obstacles. For frequencies below 400 MHz, the proportion of correct azimuth is less than 80% for obstacles on the vehicle and less than 90% for some obstacles out of the vehicle. For the second vehicle, a proportion of 99% of correct azimuths is observed. The error induced by disturbing elements is more significant for low frequencies. This can be explained by the decrease of the dimension of the DFA

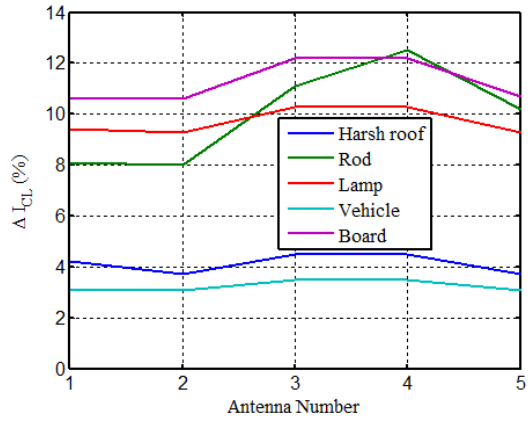

Figure 11. Comparison of simulated received current ratios at the output of DFA for different types of obstacles according to the R_{xi} antenna number.

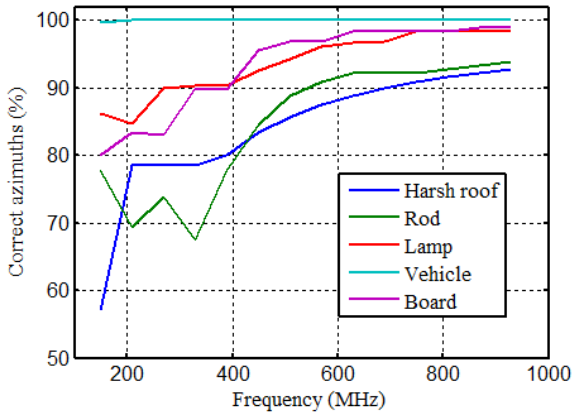

Figure 12. Proportion of correct azimuths for a SNR of 25 dB.

array in terms of wavelength in the expression of Cramer Rao Bound [17]. The frequency selectivity of the obstacle is also observed for obstacles present on the vehicle. For the rod and harsh roof, there is resonance phenomenon which amplifies the coupling between DFA and the obstacle and causes a degradation of the performance of the goniometer. Contrariwise, this phenomenon is less significant for obstacles 10 m behind the vehicle (roundtrip of the signal).

5.4. Relation between Monitoring Mode and DF Mode

Table 2 shows the ratios between monitoring (Δ_{OMS}) and DF modes ($\Delta_{I_{FF}}$) for different kinds of obstacles averaged over the frequency band 150 MHz–400 MHz and 400 MHz–1 GHz, respectively. The results show that there is a quite good correlation between ratios of monitoring mode and those of DF mode. For large deviations on the OMS monitoring mode, the proportion of correct azimuths is smaller. The ratios on the frequency band 150 MHz–400 MHz are more significant. As we can see, the degradation of the performance of DF mode is correlated with the observables of the monitoring mode (disturbance of the first OMS modulation harmonic). For example, for the two analyzed frequency bands (Table 2) the disturbance of the monitoring mode in the presence of the rod is maximal and corresponds to less accurate DF mode (proportion of correct azimuths $< 74.6\%$ for 150 MHz–400 MHz and $< 89.2\%$ for 400 MHz–1 GHz). For this reason, we pretend to detect the disturbing elements by this system, which hinder the nominal operation of the goniometer. The measured variations of the near field are correlated to the degradation of the performance of DF system.

6. DIMENSIONING OF THE PROPOSED MONITORING SYSTEM

Based on the foregoing study, the OMS technique is an effective approach for embedded antenna monitoring. Its efficiency is mainly due to an optimal tradeoff between low disturbing during the DF mode and sufficient sensitivity during the monitoring one. In order to have an idea of the performance of a complete DFA monitoring, the following settings are considered (Table 3).

The worst case for the sensitivity, obtained at 300 MHz, is considered:

- For an input power of +20 dBm, the scattered power by the OMS probe is −80 dBm, resulting in a coupling of −100 dB.
- The noise floor N for the receiver is computed with:

$$N = k.T.B.NF$$

Table 2. Relation betwen monitoring mode and DF mode in the frequency band 150 MHz–1 GHz.

Obstacle	Monitoring mode		DF mode			
	$\Delta_{OMS}(\%)$		$\Delta[I]_{CL}(\%)$		Proportion of correct azimuths (%)	
Frequency Band	150 MHz–400 MHz	400 MHz–1 GHz	150 MHz–400 MHz	400 MHz–1 GHz	150 MHz–400 MHz	400 MHz–1 GHz
Rod	3.4%	2.6%	5.6%	3%	74.6%	89.2%
Harsh Roof	2.7%	1.4%	2%	1.3%	73.3%	91.2%
Board	1.7%	1.8%	4.2%	4.1%	85.2%	97.9%
Lamp	0.4%	0.2%	3.1%	1.9%	88.3%	96.6%
Vehicle	0.5%	0.4%	1.3%	1.2%	99%	99%

Table 3. Considered parameters for the dimensioning.

Settings	Value
$p_{e_{Tx}}$: Input power	+20 dBm
n_f: Number of sampled frequencies	120 points
DFA frequency bandwidth	1.2 GHz
n_s: Number of monitoring OMS probes	18 probes
T: Measurement duration per point	0.01 s

where k is the Boltzmann's constant ($1.38 \times 10 - 23\,\mathrm{J/K}$), T the thermodynamic temperature (290 K), NF the receiver noise figure ($NF = 4\,\mathrm{dB}$) and B the spectral resolution bandwidth ($B = 100\,\mathrm{Hz}$ for a measurement rate of 100 points/s). For these values, N is equal to $-150\,\mathrm{dBm}$. The developed system must be able to measure power variations ΔP_r of 1% (which corresponds to $-20\,\mathrm{dB}$ offset) to detect perturbations from obstacles. The obtained SNR on ΔP_r is equal to 50 dB (worst case) (Fig. 13).

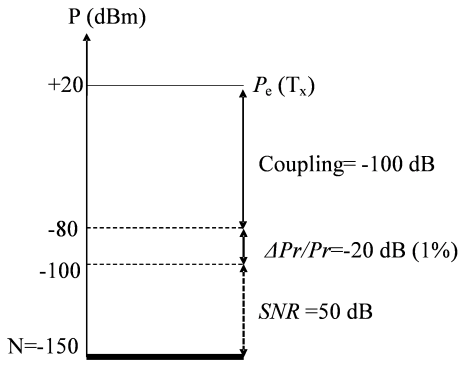

Figure 13. Power Budget for the monitoring system.

With these settings, we are able to make a monitoring of the DFA in 21.6 s ($n_s\ n_f\ T$). This monitoring process may be repeated for each new configuration of the carrier or periodically if the context is uncontrolled.

7. CONCLUSION

This work addresses the problem of in-situ antenna monitoring for DF application. To our knowledge, there is no system able to monitor quasi continuously the validity of the DF calibration table. The ultimate goal of this study is to detect and if possible to compensate the perturbations of the antenna behavior placed in uncontrolled environment. This paper focuses on three main areas:

- An analysis at the system level of the influence of a biased calibration for DFA.
- A design of OMS probes array for antenna radiation monitoring and its partial experimental validation to detect a close scatterer.
- The correlation between the variations of the measured signals for the monitoring mode and for the DF mode.

First, the benefit of an in-situ monitoring system is demonstrated with a model combining EM simulations and antenna processing. The effect of a biased calibration is analyzed quantitatively in the following cases: strong integration on the carrier and variable obstacles. Two major requirements have to be considered in order to provide accurate measurements: minimum disturbance of the field under test and operation over a wide band of frequencies (typically two decades in DF application). The second point of the study concerns OMS technique implementation. A model that predicts the OMS scattered power is developed to set the configuration (optimal probe length ...). The presence of nearby (up to 90 cm distance) metallic rod perturbing nominal configuration is detected by measuring the variation of the OMS scattered field by the probe with received power variation larger than 5%. Finally, an overall design of the system shows that it is possible to measure variation in the order of 1% of the coupling between auxiliary antenna and DFA with a SNR of 50 dB for a transmitted power of 0.1 W and measuring time of 0.01 s per sample point leading to a global measurement time less than 22 s. This study has focused on DF application, but the proposed in-situ monitoring system can also find great potential in other applications where antenna radiation characteristics are critical for the application (radar, radio navigation ...).

ACKNOWLEDGMENT

The authors would like to thank the DGA for funding a part of this study and Mervi Hirvonen from VTT, Finland for the collaboration on OMS platform design.

REFERENCES

1. Tunker, T. and B. Friedlander, *Classical and Modern Direction-of-Arrival Estimation*, Academic Press, 2009.
2. Bellion, A., et al., "Calibration of direction finding antennas in complex environment," *Colloque URSI*, Chicago, USA, 2008.
3. Gupta, I. J., et al., "An experimental study of antenna array calibration," *IEEE Trans. Ant. and Propag.*, Vol. 51, No. 3, 664–667, 2003.
4. Infante, L., S. D. Quintili, and C. Romanucci, "A real-time diagnostic tool for phased array antenna systems," *IEEE International Symposium on Phased Array Systems & Technology*, 725–730, 2013.
5. Zarbouti, D., et al., "The effective radiation pattern concept for realistic performance estimation of LTE wireless systems," *International Journal of Ant. and Propag.*, 2013.
6. Bolomey, J. C. and F. E. Gardiol, *Engineering Applications of the Modulated Scatterer Technique*, Artech House, 2001.
7. Cullen, A. L. and J. C. Parr, "A new perturbation method for measuring microwave fields in free space," *Proceedings of the IEE — Part B: Radio and Electronic Engineering*, Vol. 102, No. 6, 836–844, 1955.
8. Lao, R. R., et al., "Optically modulated scatterer technique for radiation pattern measurement of small antennas and RFID tags," *Antennas and Wireless Propagation Letters*, Vol. 8, 76–79, 2009.

9. Pursula, P., et al., "Antenna effective aperture measurement with backscattering modulation," *IEEE Trans. Ant. and Propag.*, Vol. 55, No. 10, 2836–2843, 2007.
10. Liang, W., et al., "The use of an optically modulated scatterer to measure the performance of microwave electromagnetic wave absorber," *2002 3rd International Symposium on Electromagnetic Compatibility*, 404–407, 2002.
11. Choi, J. H., B. Y. Park, and S. O. Park, "Source location estimation using phaseless measurements with the modulated scattering technique for indoor wireless environments," *Progress In Electromagnetics Research C*, Vol. 14, 197–212, 2010.
12. Ostadrahimi, M., et al., "Enhancement of near-field probing in a microwave tomography system," *Antennas and Propagation Society International Symposium (APSURSI)*, 1–2, 2012.
13. Memarzadeh-Tehran, H., J. Laurin, and R. Kashyap, "Optically modulated probe for precision near-field measurements," *IEEE Trans. Inst. and Meas.*, Vol. 59, No. 10, 2755–2762, 2010.
14. Ghattas, L., et al., "Benefit of a monitoring system in-situ for direction finding antennas," *35th AMTA)*, 2013.
15. Fikioris, G. and C. A. Valagiannopoulos, "Input admittances arising from explicit solutions to integral equations for infinite-length dipole antennas," *Progress In Electromagnetics Research*, Vol. 55, 285–306, 2005.
16. Fikioris, G. and T. T. Wu, "On the application of numerical methods to Hallen's equation," *IEEE Trans. Ant. and Propag.*, Vol. 49, No. 3, 383–392, 2001.
17. Bellion, A., et al., "Application de la borne de Cramer Rao dans le cas des systmes antennaires complexes de goniomtrie," *Colloque GRETSI*, 1053–1056, 2007.
18. http://www.enablence.com/media/mediamanager/pdf/32-enablence-datasheet-ocsd-pd-pin1310-1550-pdcs30t-18ghz-ingaas.pdf.
19. Ghattas, L., et al., "Broadband optically modulated scatterer probe for near field measurements," *35th AMTA*, 2013.
20. Pursula, P., et al., "Backscattering-based measurement of reactive antenna input impedance," *IEEE Trans. Ant. and Propag.*, Vol. 56, No. 2, 469–474, 2008.
21. Bories, S., "Small antennas impedance and gain characterization using backscattering measurements," *Proceedings of EuCAP*, 1–5, 2010.
22. Yaghjian, A. D., "An overview of near-field antenna measurements," *IEEE Trans. Ant. and Propag.*, Vol. 34, No. 1, 30–45, 1986.